Calibration of CT Hounsfield units for radiotherapy treatment planning of patients with metallic hip prostheses: the use of the extended CT-scale

2003 Phys. Med. Biol. 48 1591

(http://iopscience.iop.org/0031-9155/48/11/308)

INSTITUTE OF PHYSICS PUBLISHING PHYSICS IN MEDICINE AND BIOLOGY

Phys. Med. Biol. **48** (2003) 1591–1603 PII: S0031-9155(03)58704-8

Calibration of CT Hounsfield units for radiotherapy treatment planning of patients with metallic hip prostheses: the use of the extended CT-scale

C Coolens and P J Childs

The Joint Department of Physics, Institute of Cancer Research and Royal Marsden NHS Trust, Sutton, SM2 5PT, UK

E-mail: Catherine.Coolens@icr.ac.uk

Received 23 January 2003
Published 20 May 2003
Online at stacks.iop.org/PMB/48/1591

Abstract

Heterogeneity corrections for radiotherapy dose calculations are based on the electron density of the disturbing heterogeneity. However, when CT planning a radiotherapy treatment, where metallic hip implants are present, considerable artefacts are seen in the images. Often, an additional problem arises whereby no information regarding the artificial hip's composition and geometry is available. This study investigates whether the extended CT range can be used to determine the composition (hence electron density) of artificial hips in radiotherapy patients. Two CT-calibration methods were evaluated, one based on material substitution, the other a stoichiometric calibration. We also evaluate whether the physical dimensions of metal prostheses can be accurately imaged for subsequent use in treatment planning computers. Neither calibration method successfully predicted electron densities. However, the limited range of implant-materials used in patients means that the extended CT range can still successfully distinguish between implant densities. The physical dimensions can be determined to ± 2 mm by establishing the required windowing of displays for each material. The cross-sectional area of the prosthesis and the presence of other high-density objects in a CT slice can influence the generated CT number and careful design of calibration phantoms is essential.

1. Introduction

Total hip replacements have become a common procedure (Hazuka *et al* 1988) and this is reflected in the number of patients with hip replacements presenting for radiotherapy (RT) treatment of pelvic cancers. The aim of radiotherapy treatment planning is to deliver a homogeneous dose of radiation to an accurately localized tumour volume with minimal effects

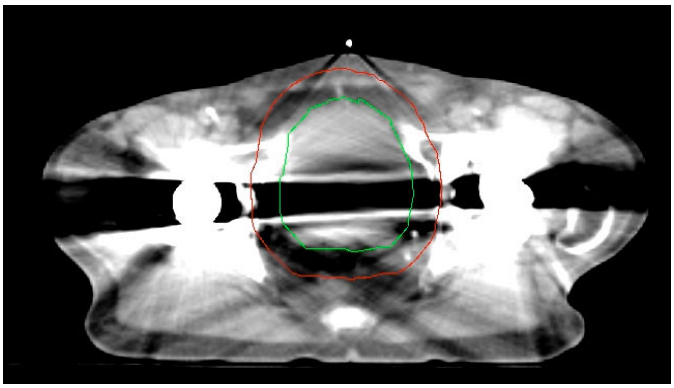

(a)

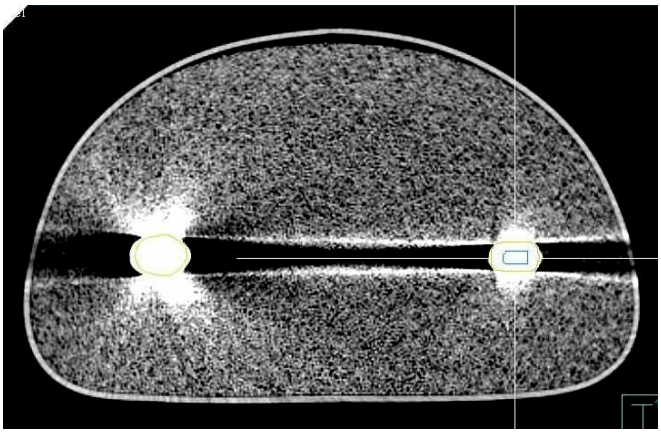

(b)

Figure 1. CT images of (a) pelvic scan of patient with bilateral hip replacements. The inner contour represents the bladder volume; the outer one represents the planning target volume; (b) pelvic shaped phantom filled with Lincolnshire bolus and containing two artificial implants displayed with a CT windowing for normal tissue.

on the surrounding normal tissue. Hip prostheses consist of materials that have higher atomic numbers and are much denser than any human tissue, and where beams pass through the implant they shadow the target volume and affect the dose distribution. In the case of single hip prostheses it may be possible to avoid the prosthesis by using a non-standard planning technique. However, for bilateral prostheses, this is often not an option because the constraints on beam geometry could compromise target volume coverage and increase the dose to organs at risk.

Various authors have investigated the effects of a single hip replacement on the dose distribution behind the hip (Hudson *et al* 1984, Biggs *et al* 1988, Erlansson *et al* 1991, Sibata *et al* 1990, Hazuka *et al* 1988, 1993, Carolan 2000, Eng 2001). Only Burleson (1991) and Alecu *et al* (1999) have discussed the effects on the dose distribution due to bilateral hip replacements.

When planning radiotherapy treatments based on computed tomography (CT) scans with bilateral metallic implants, considerable artefacts associated with the prostheses are seen in

the images. An example of such a CT scan is given in figure 1 and clearly shows the two most significant types of artefacts. Firstly there are bright straight lines that arise across the image (called streaks), and secondly dark banding between both implants. The large quantities and amplitudes of the streaks can degrade the image so much that it is either unreadable or that no reliable outlining is possible. Several effects come into play and if not directly responsible for the artefact, they will contribute to the overall degrading of the image (Goldman and Fowlkes 1995). The most severe result of CT scanning metallic prostheses is the production of incomplete data or gaps when the attenuation of the photon beam was so strong that almost no photons reached the detector (photon starvation). As a result of this, the dynamic range of the CT scanner stretches to its lower limit, which is then back projected into the image. This results in two effects. First of all, these so-called 'hollow' projections produce lower CT numbers of the implants since a relatively lower attenuation is registered. Secondly, the artefacts will be accompanied by structured noise, which can be seen as bright borders surrounding the artefact. (Throughout this text we use CT values in units of CT numbers, which are the Hounsfield number (HU) plus 1000; i.e. 0 = air, and 1000 = water.)

These artefacts lead to two problems: outlining the hips or regions of interest and obtaining the correct electron density of the prostheses (Ding *et al* 2001, Roberts 2001, Carolan *et al* 2000, Alecu *et al* 1999). An additional problem exists because quite often there are no records of the patient's type of hip prosthesis, i.e. its shape, material and density.

In the last 10–15 years the problem of artefacts in CT has been increasingly investigated. Generally, solutions for partial volume effects and beam hardening have become quite standardized on the more recent CT scanners (Jospeh 1978).

Several approaches have been developed to try to reduce artefacts due to missing data in CT scans containing metallic objects. Generally this can be achieved in three ways. The easiest method is imaging less attenuating objects which involves avoiding or at least reducing the generation of the missing data (Robertson *et al* 1988, 1989, Seitz *et al* 1985). A second way is by increasing the effective energy of the x-ray beam, but this is limited by technical problems in generating the x-ray beam. The third and most sophisticated method of reducing metallic artefacts is by artificially generating values for the missing data and then reconstructing the image (Fishman *et al* 1986). However, although these mathematical algorithms may have the potential of producing high quality images, none of the suggested approaches has been applied to clinical routine yet because their computational performance is not as good as filtered back projection.

The only exception to this is the use of the extended CT-scale. This is a different approach to the problem of metallic artefacts, which is available on the more recent Siemens scanners and has been developed by Klotz *et al* from Siemens Medical Systems. The principle is, that by scaling down the CT numbers by a factor of 10, the CT-scale is expanded from −10 240 to 30 710 HU. Metals with CT numbers of about 20 000–30 000 HU can produce artefacts of several thousand HU and both hip implant and artefact can exceed the limits of the standard CT-scale. By scaling down the HU however, one can differentiate between the metal and its surroundings. Although there is some loss in contrast resolution, the algorithm allows detailed geometric information to be preserved and the metallic objects to be outlined correctly, which is also reported by Klotz *et al* (1990), who tested their technique on a Ti-alloy hip implant and by Link *et al* (2000).

For photon therapy, the accuracy of dose calculations based on CT data is partly determined by the precision of the calibration of CT numbers to relative electron density. This relationship can be used, provided that the Compton process is the predominant interaction. The error in the final electron density distribution depends on various sources such as the type of scanner, variation between measurements, location of the object in the image (Schneider *et al* 1996).

For most soft tissues, the effective atomic numbers are close to that of water. For metallic implants however, the effective atomic number is quite different and may vary from 21.7 for Ti-alloy to 27.7 for Co–Cr–Mo. Hence, it is not evident that a CT number is sufficient to determine the electron density for materials significantly denser than bone.

Using the extended CT number algorithm we have examined the three most common hip prosthesis materials, i.e. titanium-alloy (Ti), stainless steel and cobalt–chromium–molybdenum (Co–Cr–Mo) alloy (BS EN 1998). Without using the extended CT-range, all these samples would appear with identical CT numbers, e.g. the maximum value of 3071 on our CT scanner. A calibrated extended CT number image should allow a correct electron density/physical density to be entered in the treatment planning system (TPS), facilitating an accurate dose calculation in the presence of hip prostheses if the TPS algorithm can utilize the information accurately. Ding *et al* (2001) recently calculated dose inhomogeneity correction factors for beams passing through metal prostheses and compared the results of Monte Carlo simulation with those predicted by the ratio of TPR (tissue phantom ratio) method. They showed that the simpler ratio of TPR method could adequately predict inhomogeneity dose correction factors when the physical density of the metal implant is used in obtaining the water-equivalent depth.

2. Methods and materials

We have investigated two methods of producing a CT-calibration table for metallic materials.

The first method is an extension of an early report on electron density corrections for bone inhomogeneities (Henson and Fox 1984). The idea behind this is to test whether the CT numbers measured in the extended CT-scale can actually give correct electron densities. A range of readily available metals of known composition was used for this method, rather than just those used in hip prostheses. The measured CT numbers of the variety of metal substitutes were used to calculate their electron density. This was then compared with the electron density calculated from the elemental composition of the materials. This would allow us to both verify this method and produce a calibration table that can be put in to the treatment planning system.

The second method is a stoichiometric calibration, in which both the measured CT numbers and chemical composition of these test metals are used to predict the CT numbers of the real hip implant materials. This technique is an extension of that described by Schneider *et al* (1996), who tested their method for a range of soft tissue substitutes. By fitting the dependence of the photon attenuation as a function of the atomic number of the elemental composition of these materials, the response of the CT unit can be parametrized. This is then used to compare calculated and measured CT numbers for a real hip implant material.

2.1. Calculation of electron density using the atomic composition

To calculate the electron densities of the various hip prostheses and test materials, their chemical compositions were taken into account, using

$$\rho_e = \rho N_A \sum \frac{w_i Z_i}{A_i} \tag{1}$$

where ρ is the physical density, N_A is Avogadro's number ($= 6.022\,045 \times 10^{23}$ mol^{-1}), Z_i and A_i are the atomic number and atomic weight of the ith element and w_i is its proportion by weight. The relative electron densities were then obtained by dividing the electron densities of the material by that of water.

2.2. Method 1—calculation of electron density using CT numbers based on Henson's method

A way to describe the attenuation caused by metallic implants is to consider the mass attenuation coefficient (in $cm^2\ g^{-1}$) (Henson and Fox 1984).

For an element of atomic number Z and atomic weight A, which intersects an x-ray beam of effective energy E keV, this may be written as

$$\mu(E)/\rho = Cf(Z, E) \tag{2}$$

where

$$C = 10^{-24} N_A/A \text{ (in cm}^2 \text{ atom}^{-1} \text{ barn}^{-1}) \tag{3}$$

with N_A Avogadro's number and $f(Z, E)$ the atomic cross-section of the element at energy E (barns/atom).

By incorporating the electron density of water and relationship (1), the relative electron density of the material is

$$\rho_e^w = 2.9968\mu_w(E)\left(\frac{N_m - N_a}{N_w - N_a}\right)\frac{Z^*}{f(Z^*, E)} \tag{4}$$

where N_m, N_w and N_a are the CT numbers of the material, water and air respectively. Z^* is the effective atomic number of the compound.

Based on a comparative analysis of the various ways of calculating the effective atomic number (Henson 1983), the following method was chosen to determine the effective atomic number of the compounds:

$$Z^* = \left[\sum_i \left(a_i {Z_i}^n\right)\right]^{1/n} \tag{5}$$

with $n = 3.4$ (Weber *et al* 1969).

Calculation of function $f(Z, E)$ was done according to Henson (1983).

2.3. Method 2—stoichiometric calibration

A CT image represents a matrix of photon attenuation coefficients.

For a material at a specific position along the projection line, the linear attenuation coefficient is

$$\mu(E) = \rho N_A \sum_{i=1}^{n} \frac{w_i}{A_i}\sigma_i(E) \tag{6}$$

where ρ is the physical density (g cm^{-3}), N_A is Avogadro's number ($6.022\,045 \times 10^{23}$ mol^{-1}), A_i is the atomic weight of the ith element, w_i is its proportion by weight and σ_i the total cross-section (barn/atom).

A direct calculation of the CT number using the equations above, together with the tabulated values for the cross-sections σ, is not possible because the spectrum is unknown. For diagnostic x-ray energies however, a good parametrization of the cross-sections is given by Rutherford *et al* (1976):

$$\sigma_i(E) = Z_i K^{KN}(E) + {Z_i}^{2.86} K^{sca}(E) + {Z_i}^{4.62} K^{ph}(E). \tag{7}$$

In the first term of this formula, K^{KN} denotes the Klein–Nishina coefficient. The second term describes coherent scattering and the photoelectric absorption is taken into account by the

Table 1. Composition, physical density and relative electron density of the three most commonly used types of hip prosthesis evaluated.

Element	Ti-alloy	Stainless steel	Co–Cr–Mo alloy
(a) Composition (in w)			
Aluminium	0.055–0.068	–	–
Titanium	Balance	–	–
Vanadium	0.035–0.045	–	–
Silicon	–	0.0075 max	<0.01
Iron	0.003 max	Balance	<0.01
Oxygen	0.002	–	
Carbon	0.0008 max	<0.001	<0.0035
Manganese	–	0.028–0.043	<0.01
Phosphorus	–	0.00025 max	–
Sulphur	–	0.0001 max	–
Cobalt	–	–	Balance
Chromium	–	0.2–0.22	0.265–0.3
Nickel	–	0.08–0.1	<0.0075
Molybdenum	–	0.02–0.03	0.045–0.07
Nitrogen	0.0005 max	0.0035–0.005	–
(b) Physical density (g cm^{-3})	4.48	6.45	8.2
(c) Relative electron density			
Average	3.71	5.39	6.76

third term. If $\sigma_i(E)$ is eliminated in equation (6) by this expression, then the mean value of the attenuation coefficient, relative to water will be

$$\frac{\overline{\mu}}{\overline{\mu_{H_2O}}} = \frac{\rho}{\rho_{H_2O}} \frac{\sum_{i=1}^{n} (w_i/A_i)\left(Z_i + {Z_i}^{2.86}k_1 + {Z_i}^{4.62}k_2\right)}{(w_H/A_H)(1+k_1+k_2) + (w_O/A_O)(8+8^{2.86}k_1+8^{4.62}k_2)} \tag{8}$$

with $k_1 \equiv \overline{K}^{sca}/\overline{K}^{KN}$ and $k_2 \equiv \overline{K}^{ph}/\overline{K}^{KN}$.

The CT numbers of four test materials of known chemical composition (listed in table 2) were measured with a fixed energy of 140 kV. Then, the values of the coefficients were determined by carrying out a least-squares fit of the measured CT numbers to equation (8). This can be seen as a parametrization of the CT unit with resulting values of 1.13×10^{-4} and 9.87×10^{-7} for k_1 and k_2. By means of equation (8), the definition of the HU and the values of (k_1, k_2) the CT numbers of the real hip prostheses were then calculated.

2.4. Experimental procedure

The scanner used in all phantom measurements was a third generation Siemens Somatom 4Plus. The scan parameters used for the calibration were 140 kV, 256 mAs. Axial scans were performed with a slice width of 5 mm and with the test materials placed in a 40 ×40 ×40 cm Perspex walled, water filled phantom, 5 cm under the water surface. Details of the implant samples are listed in table 1, together with their physical densities, electron densities relative to water and compositions as supplied by the manufacturers. Two types of Ti-alloy prosthesis were tested, provided by different companies. Their compositions were similar, the relative electron densities deviating by no more than 1%. The mean CT-value of the core region of the samples was used as visualized in a tranverse slice with a signifcant cross-sectional area (figure 2 shows a typical core region dimension for a hip sample). To investigate the effects of the presence of more than one dense object in a transverse scan, a titanium implant was scanned alongside samples of dural, mild steel and copper (figure 4(a)). A transverse scan

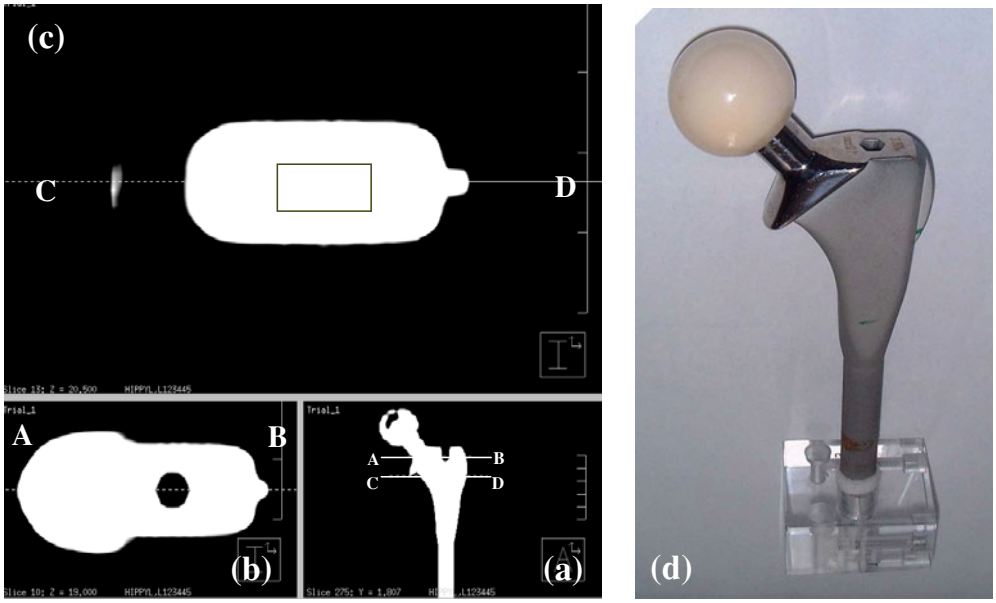

Figure 2. CT images of the JRI Ti implant: (a) coronal view indicating the positions of the transverse slices in (b) and (c). Figure (c) also shows the core region of interest selected to identify the implant. The windowing has been selected to reproduce the known dimensions of the implant; (d) photograph of the CT imaged Ti implant. The ceramic head is a hollow sphere, which results in an air cavity at the end of the metal pin.

of a Co–Cr–Mo, Ti-alloy and stainless steel prostheses was made, then repeated with the phantom rotated 90° to observe the significance of increasing the cross-sectional areas from approximately 1 to 6 cm^2 in the normal patient orientation to 16–30 cm^2.

2.5. CT windowing

Measurements of all CT numbers were performed within the ADAC Pinnacle TPS Versions 5.2g-6.2b (Milpitas, USA) by windowing to the CT numbers in the core of the hip. The core region of the prosthesis (figure 2) was used to identify the material. Then the CT number windowing was adjusted on the TPS so that the visual dimensions matched the measured dimensions of the prosthesis.

3. Results and discussion

3.1. Method 1—calculation of electron densities with measured CT numbers

The test materials, together with their relative electron density (both theoretical and calculated), measured CT number, effective atomic number and physical density are listed in table 2. This clearly shows that the calculation of the relative electron density using these CT numbers did not agree with the theoretical electron density. Deviations between both values ranged from 40 to 340% for brass and stainless steel. Nevertheless, it must also be noted that the CT measurements were obtained with an uncertainty of up to 16% for stainless steel. The errors tabulated for the calculated electron densities show the influence of this CT number

Table 2. Effective atomic number, relative electron density calculated from atomic composition density of test metals in method 1, theoretical electron density, measured CT number, physical density.

Test material	Z_{eff}	ρ_e^w (calc)	St. dev. ρ_e^w (calc) (%)	ρ_e^w (theor)	Meas_CT number (HU)	St. dev. CT number (%)	ρ (g cm^{-3})
Copper	29.0	7.48	11.19	7.35	5566	13	8.96
Stainless steel	25.6	22.52	5.16	6.56	11 847	16	7.84
Brass	34.1	2.69	9.2	6.78	6861	11	8.36
Mild steel	26	14.76	11.31	6.54	7976	13	7.8

uncertainty and indicate that only for copper there is an agreement between calculated and theoretical electron density. It is thought that the discrepancy between the theoretical and calculated electron density is caused by a combination of approximations in the method. First of all, there is the assumption of a linear relationship between the CT number and the electron density. Although this is true for most soft tissues or even soft bone, it is likely that for higher Z materials the CT number cannot estimate the electron density accurately enough due to the larger influence of the photo-electric effect at the typical CT energies (70–80 keV). Secondly, failure to calculate the electron density might be caused by the approximation of the cross-section data. Basic cross-section data have been tabulated for a number of energies (Veigele *et al* 1973) and functions to fit these points have been published (Rutherford 1976). Application of these formulae, however, to higher Z elements (starting from bone) reveals discrepancies from published data. An attempt was made by Henson (1983) to improve the interpolation of attenuation coefficients over an atomic number range of 1–30. This approach was used in this study and should cover even the highest effective atomic number used here (Co–Cr–Mo, $Z_{\text{eff}} = 27.6$). These equations allow calculation of attenuation coefficients to a good agreement with published data for energies between 50 and 100 keV. In the present case however, the solid high-Z material substitutes possibly cause a fair amount of beam hardening and increase the effective energy of the beam significantly. Additionally, the large differences between actual and calculated electron densities could be the result of both the reconstruction effects and CT calculations on the scanner. Hence if the discrepancy is not caused by the CT measurements then Monte Carlo simulation would be the only way to obtain a more accurate picture of the cross-section data for high-Z materials and hence, the artefacts aside, electron density.

3.2. Method 2—stoichiometric calibration

Results of the CT measurements of the real hip prostheses are given in table 3, together with the calculated CT numbers and the relative electron densities. A plot of both measured and calculated CT numbers versus relative electron density is given in figure 3, as well as the usual CT range for soft tissue.

The bilinear dotted line represents the actual calibration curve. This was done to overcome the small number of data points within the wide range of CT numbers between approximately 7300 for Ti to 14 800 for Co–Cr–Mo. The discrepancy between the calculated and measured CT numbers indicates that even the stoichiometric technique cannot provide a useful calibration curve. Although this type of calibration, based directly on tissue substitutes, is very sensitive to the particular substitutes chosen for the measurement, it is unlikely that this would explain the large difference between measured and calculated CT numbers. An indication of why this method fails probably lies within the k_1 and k_2 factors, i.e. the ratios of the partial interaction

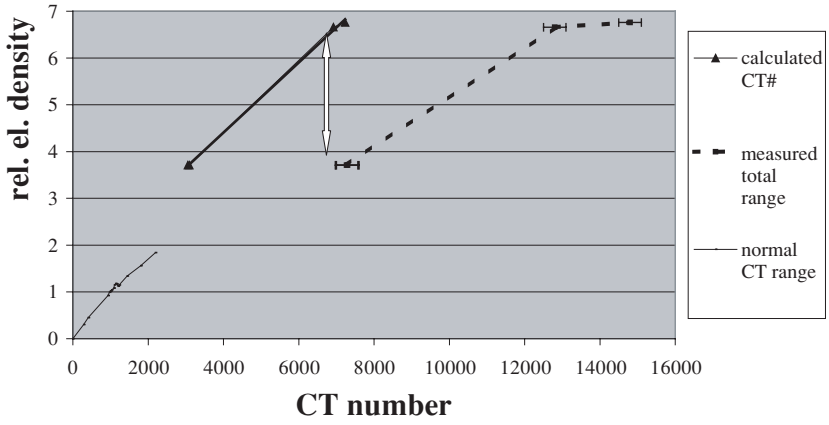

Figure 3. Calibration table with calculated and measured CT numbers in the extended CT range. The solid line connects the calculated numbers; the broken line connects the measured numbers.

Table 3. Relative electron density, calculated CT number, measured CT within the TPS for the prostheses evaluated along with the windowing requirements to visualize actual dimensions of the implants.

	ρ_e^w	Calculated CT no	Measured CT no	Window width	Window level
Ti (JRI[a])	3.71	3091	7271	200	3000
Ti (DePuy[a])	3.66	3054	7300	200	3000
Stainless steel	5.39	6918	12 800	200	7720
Co–Cr–Mo	6.76	7233	14 800	200	8000

[a] Different manufacturers of hip prostheses.

coefficients. Comparing these factors with the theoretical ratios for the different materials at 80 keV (Hubbell *et al* 1986) indicates that the k_1 and k_2 factors are much smaller than theoretically established. For titanium for example k_1 and k_2 are respectively of the order of 10^{-1} and 10^0 at 80 keV whereas the values obtained here (section 2.3) are much lower. The stoichiometric method attempts to 'match' the cross-sections for this particular energy and materials to the measured CT numbers. The fact that this comparison underestimates k_1 and k_2 arises from the overestimation of the Compton interaction which in turn is due to the hollow projections behind the hip material. In other words, the attenuating effect of the high-Z material is so severe (resulting in a significant increase in effective beam energy) that the calibration tries to compensate for this by assigning k_1 and k_2 with a larger contribution from Compton interactions since this is the dominant interaction at energies above 150 keV. This method could therefore only be accurate if the CT scanner was able to correct for the severe beam hardening due to the metal prostheses.

A fortunate feature of clinical hip materials, however, is the variation of measured CT numbers with relative electron density. Regardless of the bilinear fit that was made to the data points in figure 3, one can see that the difference in CT numbers between the various types of hip prostheses is large, with approximately 2000 HU separating Ti alloy from stainless steel, and stainless steel from Co–Cr–Mo alloy. Hence, by defining threshold values that divide the scale of CT numbers into different groups, a determination of the implant material is possible.

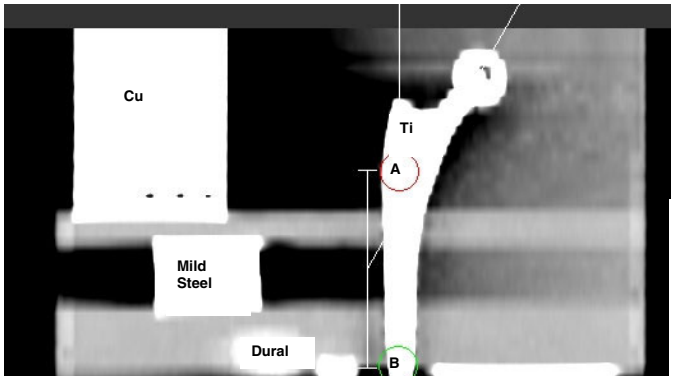

(a)

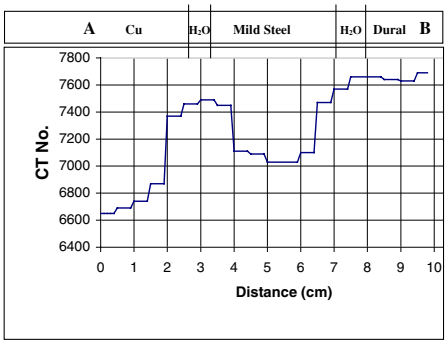

(b)

Figure 4. (a) Reconstructed CT image plane through Ti hip and several metal samples; (b) plot of CT number through the centre of the Ti hip prosthesis showing the effect of adjacent metal structures and cross-sectional area of the hip.

3.3. Practical implementation

Known samples of titanium, stainless steel, and Co–Cr–Mo alloy can be used for two purposes. Firstly the CT numbers can be determined for each material generated by the CT scanner using the standard scan parameters locally employed. Secondly, the windowing on the TPS can be adjusted for each material so that the image of the metal sample matches the actual dimensions. This windowing can then be selected once the material is identified in a patient CT image, and the actual dimensions based on the visible image of the implant. The CT window width and level that correspond with the measured dimensions of stainless steel, Co–Cr–Mo and Ti alloy hips are listed in table 3.

Different window widths/levels were required for each material evaluated, but having established the appropriate levels, the actual dimensions could be accurately outlined on subsequent transverse scans to within 2 mm as a region of interest (ROI) within the TPS. The ROI may then be assigned the correct relative electron density or physical density (depending on the requirements of the TPS calculation algorithm).

Where two high-density samples are present on a single scan slice, the shift in titanium CT number is not significant enough to inhibit identification (typically 13%). This is shown in the CT number profile in figure 4(b) taken along the centre of the titanium implant where the titanium prosthesis was scanned with samples of brass, mild steel and dural in a water

Table 4. Variation of mean core CT number with range of cross-sectional areas of the implant containing the core ROI.

Material	Cross-sectional area (cm^2)	CT number
Ti (DePuy)	2–6	7340
Ti (DePuy)	16	3900
Co–Cr–Mo	1–4	14 100
Co–Cr–Mo	18	6620
Stainless steel	1–4	13 340
Stainless steel	30	5380

tank. The copper and mild steel significantly affect the titanium CT numbers (decrease), while the dural has negligible effect. Two slices in the set contain water and titanium only (the remaining have partial metal/water content thus explaining the gentle transition between slices seen in the profile). For these slices there is a small difference in titanium CT number seen of approximately 2% due to the variation in cross-section of the titanium implant from 2.8 cm^2 to 2.0 cm^2.

Care should be taken in the design of the calibration phantom since large cross-sectional areas in the transverse plane will cause a shift in the CT number compared to the relatively small cross-sectional areas found in patient implants. Table 4 shows the effect of increasing the cross-sectional area of the implant material.

4. Conclusion

A possible calibration method could only be established using the measured CT numbers and the elemental compositions of the test materials (stoichiometric method). Nevertheless, further work will be required on the reduction of metal induced artefacts in computed tomography and the interpolation of atomic cross-section data (Monte Carlo calculations) in order to confirm whether this is indeed a useful calibration technique. However, it can be argued whether this would be necessary considering the small number of implant materials commonly used, each having rather distinct CT numbers. To produce a calibration curve, scanning of various samples of real hip prostheses and test materials would be required. Considering the variations in CT numbers using different CT scanners and imaging factors (kV, mAs), it might be desirable for a phantom to be made incorporating different samples of known implant material. This could allow the electron density of the prosthesis to be determined and inhomogeneity corrections to be made in the radiotherapy treatment plan.

An extended CT scale CT scan performed on a patient can therefore be used to establish whether the prostheses present are ‘high-density’ (Co–Cr–Mo or stainless steel), or ‘low-density’ (titanium) and therefore enable the user to manually assign an approximate density/electron density. The physical dimensions of the patient prosthesis can first be established by appropriate windowing of the CT image and manually outlining the structure on the TPS. The manually outlined structure can then be assigned a density/electron density for the material in order to produce more accurate dose distributions.

Acknowledgments

We are greatly indebted to Keith Jackson of JRI Ltd, London and to DePuy International Inc, Leeds who provided the data and samples of the hip prostheses. We are grateful to Christoph

Suess of the Siemens Medical Department for his comments on the CT artefacts and to Uwe Schneider of the Triemli Hospital in Zurich for his useful advise on the stoichiometric calibration. Furthermore we would like to express our appreciation to the staff of the Royal Marsden Hospital radiotherapy department for their general support and to E Castellano for her useful comments on the work.

References

Alecu R 1999 Traditional and MLC based dose compensator design for patients with hip prostheses undergoing pelvic radiation therapy *Med. Dosim.* **24** 33–7

Biggs P J and Russell M D 1988 Effect of a femoral head prosthesis on megavoltage beam radiotherapy *Int. J. Radiat. Oncol. Biol. Phys.* **14** 581–6

BS EN 1998 Document 12010:1998, Clause 6 Materials: Joint replacement implants

Burleson W D, Stutzman C D, Stitt J A, Karlsson U L and Mian T A 1991 In vivo isocenter dose in two hip prosthesis patients *Int. J. Radiat. Oncol. Biol. Phys.* **20** 1347–52

Carolan M 2000 Effect of hip prostheses on radiotherapy dose *Australas. Radiol.* **44** 290–5

Ding G X and Yu C W 2001 A study on beams passing through hip prosthesis for pelvic radiation treatment *Int. J. Radiat. Oncol. Biol. Phys.* **51** 1167–75

Eng T Y 2001 Dose attenuation through a titanium alloy hip prosthesis *Med. Dosim.* **25** 7–8

Erlanson M, Franzen L, Henriksson R, Littbrand B and Lofroth P O 1991 Planning of radiotherapy for patients with hip prosthesis *Int. J. Radiat. Oncol. Biol. Phys.* **20** 1093–8

Fishman E, Magid D and Robertson D 1986 Metallic hip implants: CT with multiplanar reconstruction *Radiology* **160** 675–81

Goldman L W and Fowlkes J B 1995 Medical CT and ultrasound: current technology and applications *Proc. 1995 Summer School on CT and US Technology and Application of the AAPM* (ISBN: 1-883526-03-5)

Hazuka M B, Ibbott G S and Kinzie J J 1988 Hip prostheses during pelvic irradiation: effects and corrections *Int. J. Radiat. Oncol. Biol. Phys.* **14** 1311–7

Hazuka M B, Stroud D N, Adams J, Ibbott G S and Kinzie J J 1993 Prostatic thermoluminescent dosimeter analysis in a patient treated with 18 MV X rays through a prosthetic hip *Int. J. Radiat. Oncol. Biol. Phys.* **25** 339–43

Henson P W 1983 Attenuation coefficient and atomic number calculation involving elements between hydrogen and zinc in the CT scanner range of 50 to 100 keV *Aust. Phys. Eng. Sci. Med.* **6** 20–5

Henson P W and Fox R A 1984 The electron density of bone for inhomogeneity correction in radiotherapy planning using CT numbers *Phys. Med. Biol.* **29** 351–9

Hubbell J H, Gerstenberg H M and Saloman E B 1986 Bibliography of Photon Total Cross Section (Attenuation Coefficient) Measurements 10 eV to 13.5 GeV *National Bureau of Standards Internal Report NBSIR 86-3461*

Hudson F R, Crawley M T and Samrasekera M 1984 Radiotherapy treatment planning for patietns fitted with prostheses *Br. J. Radiol.* **57** 603–8

Jospeh P M 1978 A method for correcting bone induced artifacts in CT scanning *J. Comput. Assist. Tomogr.* **12** 100–8

Kijewski P K and Bjarngard B E 1978 Correction for beam hardening in computed tomography *Med. Phys.* **5** 209–14

Klotz E, Kalender W, Sokiranski R and Felsenberg D 1990 Algorithms for the reduction of CT artifacts caused by metallic implants *Proc. SPIE* **1234**

Link T M, Berning W, Scherf S and Joosten U 2000 CT of metal implants: reduction of artifacts using an extended CT scale technique *J. Comput. Assist. Tomogr.* **24** 165–72

Roberts R 2001 How accurate is a CT-based dose calculation on a pencil beam TPS for a patient with a metallic prosthesis? *Phys. Med. Biol.* **46** N227–34

Robertson D, Magid D and Poss R 1989 Enhanced computed tomography techniques for the evaluation of total hip arthroplasty *J. Arthroplasty* **4** 271–6

Robertson D, Weiss P, Fishman E, Magid D and Walker P 1988 Evaluation of CT techniques for reducing artifacts in the presence of metallic orthopedic implants *J. Comput. Assist. Tomogr.* **12** 236–41

Rutherford R A, Pullan B R and Isherwood I 1976 Measurement of effective atomic number and electron density using an EMI scanner *Neuroradiology* **11** 15–21

Schneider U, Pedroni E and Lomax A 1996 The calibration of CT Hounsfield units for radiotherapy treatment planning *Phys. Med. Biol.* **41** 111–24

Seitz P and Ruegsegger P 1985 CT bone densitometry of the anchorage of artificial knee joints *J. Comput. Assist. Tomogr.* **9** 621–2

Sibata C H, Mota H C, Higgins P D, Gaisser D, Saxton J P and Shin K H 1990 Influence of hip prostheses on high energy photon dose distributions *Int. J. Radiat. Oncol. Biol. Phys.* **18** 455–61

Veigele W J 1973 Photon cross sections from 0.1 keV to 1 MeV for elements Z = 1 to Z = 94 *At. Data Tables* **5** 51–111

Weber J and van den Berge D J 1969 The effective atomic number and the calculation of the composition of phantom materials *Br. J. Radiol.* **42** 378–83